Computational modeling of electromechanical propagation in the helical ventricular anatomy of the heart

J. Marcé-Nogué[1], G. Fortuny[2], M. Ballester[3], F. Carreras[4], and F. Roure[5]

[1] Departament de Resistència de Materials i Estructures a l'Enginyeria, Universitat Politècnica de Catalunya, Terrassa

[2] Departament d'Enginyeria Informàtica i Matemàtiques, Universitat Rovira i Virgili, Taragona

[3] Chairman of Cardiology, Department of Medicine, University of Lleida, Lleida

[4] Cardiac Imaging Unit, Cardiology Department, Hospital de la Santa Creu i Sant Pau, Universitat Autònoma de Barcelona, Barcelona

[5]Departament de Resistència de Materials i Estructures a l'Enginyeria, Universitat Politècnica de Catalunya, Barcelona

Abstract

The classical interpretation of myocardial activation assumes that the myocardium is homogeneous and that the electrical propagation is radial. However, anatomical studies have described a layered anatomical structure resulting from a continuous anatomical helical disposition of the myocardial fibers. To further investigate the sequence of electromechanical propagation based on the helical architecture of the heart, a simplified computational model was designed. This model was then used to test four

activation patterns, which were generated by propagating the action potential along the myocardial band from different activation sites.

Keywords: myocardium, fibers, Helical Myocardial Ventricular Band, electro-mechanical sequence, activation, action potential, cardiac mechanics

1 Introduction

It is well established that the sequence of electrical activation of the heart starts at the septum, propagates toward the apex and then to both ventricles, and eventually ends at the base of the heart [1,2]. This sequence accounts for the electrocardiographic signal of ventricular depolarization, which is known as the QRS wave. Based on this sequence, it has been hypothesized that the apicobasal spread of the electrical activation within the subendocardium initiates the myocardial contraction sequence [3]. Thus, the sequence of mechanical contraction is hypothesized to follow an apex-to-base propagation. However, other studies have suggested a base-to-apex sequence. For example, magnetic resonance studies have shown that the initial mechanical activation takes place at two sites at the base of the heart [4] and progresses to the apex. In contrast, isotopic studies using a Fourier analysis of the ventricular blood pool revealed that the systolic ventricular motion also follows a base-to-apex sequence [5].

The classical interpretation of myocardial activation assumes that the myocardium is homogeneous and that the electrical propagation of depolarization is radial [6]. However, it has been shown that the myocardial architecture is far from homogenous. In fact, anatomical studies have described a layered myocardial architecture. In addition, the controversy regarding the anatomical disposition of the myocardial fibers [7] has

been resolved in favor of a continuous anatomical helical disposition of the myocardial fibers [3,8–10] based on the results of recent diffusion tensor magnetic resonance imaging studies [11]. Accordingly, the electromechanical wave propagation along the myocardial fibers should follow a path that follows the helical disposition of the myocardial fibers [12–14]. However, although the knowledge of cardiac mechanics has considerably improved over the last decade, the current cardiovascular textbooks do not incorporate the recent concepts on cardiac mechanics. Instead, the current textbooks emphasize the electrical aspects of the ventricular depolarization and somehow establish confusion between the initial electrification of the heart, which corresponds to the QRS wave on the surface electrocardiogram (ECG) tracing, and the electromechanical ventricular wave, which lasts almost throughout the systolic period [15,16].

Computer modeling could provide insights into these issues. However, to date, no studies have taken into account the helical myocardial anatomy. To further investigate the sequence of electromechanical propagation according to the helical configuration of the heart, a simplified computational model was designed to test how different sites of stimuli initiation can affect its propagation sequence. In spite of the currently described models, which are complexly designed to study the whole geometry of the ventricular cavity [17,18], the simple model used herein simulates the behavior of the myocardial tissue based mainly on the continuous helical fiber architecture [19,20].

2 Methods

2.1 Modeling

To design a simplified computational method, several assumptions were taken into account. Due to the rod-shaped features of the myocardial fiber cells, the electromechanical propagation takes place along the longitudinal axis in what has been

called anisotropic conduction, which corresponds to preferential conduction along one axis [21].

The morphological and functional features of the helical myocardium were used as a reference [8,10,22], and numerical computational methods were employed to recreate its behavior. These numerical methods approach the solutions of partial differential equations and are used in computational simulation in engineering, biomechanics, bioengineering, and especially computational mechanics of the heart [17,18].

The electromechanical behavior of the myocardium was considered a coupling of two parts, which are mathematically presented and largely discussed in a previous study [19]:

- the **active part** of the myocardium due to the fibers, which are modeled as a one-dimensional finite element projected in a three-dimensional space
- the **passive part** of the myocardium due to the connective tissue, which controls the tissue deformation and maintains the cardiac fibers compact.

This electromechanical model for fiber contraction has been proven successfully for ventricular architectures other than the band approach [18,23].

2.2 Active part

The action potential activates fiber contraction, and both the action potential and the contraction propagate along a longitudinal path. The action potential **u(t)** uses the Aliev-Panfilov equations and the values proposed for the different parameters [24], which allows the calculation of the current **u(t)** at every time step. The fiber contraction was modeled using the rheological model developed by Hill-Maxwell based on Huxley's theory of the sliding filaments and cross bridge [25]. These equations enable the calculation of the fiber contraction in terms of the stress and strain.

The coupling of these two mathematical models describes the active part of the myocardium and generates a propagation model of the electromechanical behavior along the fibers (Figure 1) [19].

2.3 Passive part

Biological tissues are currently modeled as hyperplastic materials [26]. However, for the purpose of simplicity, a linear elastic response was assumed for the passive part of the myocardium, which was was modeled as a three-dimensional continuum element in the present study. In particular, this element was formulated using the Finite Element Method as an isoparametric hexahedrical element of eight nodes. The connective tissue of the myocardium was treated as a quasi-incompressible, elastic, and solid material governed by a lineal stress-strain relationship in the constitutive equation (Equation 1):

$$\underline{\underline{\sigma}}_p = \frac{\partial W}{\partial \varepsilon} = \underline{\underline{D}} \cdot \underline{\underline{\varepsilon}}, \qquad (1)$$

where $\mathbf{D_{ijkl} = D_{klij} = D_{jikl} = D_{ijlk}}$ is the elasticity tensor that relates the strains $\boldsymbol{\varepsilon}$ and the stresses $\boldsymbol{\sigma}$ considering small deformations and **W** is the deformation energy. The values chosen for the parameters of the elasticity tensor were proposed and discussed by Sermesant et al. [23].

2.4 Coupling of the two parts

The interaction of the active part and the passive part in the model generated the following governing equation (Equation 2):

$$\rho \underline{\ddot{y}} - \nabla \underline{\underline{\sigma}} = 0 \quad ; \quad \underline{\underline{\sigma}} = \underline{\underline{\sigma}}_p + \sigma_c \underline{n} \otimes \underline{n} \qquad (2)$$

where $\boldsymbol{\sigma_p}$ is the passive stress of the connective tissue, $\boldsymbol{\sigma_c}$ is the active stress due to the contraction of the fiber generated by the action potential **u(t)**, **n** is the direction vector of

each fiber, ρ is the density, and $\ddot{\underline{y}}$ is the acceleration vector. The boundary conditions describing the behavior of certain fixed points observed in real images were included.

2.5 Generating a computational mesh

A mesh is a collection of vertices, edges, and faces that define the shape of a polyhedral object in 3D computer graphics and solid modeling. The faces usually consist of triangles, quadrilaterals, or other simple convex polygons that simplify and discretize the geometry to solve the equations using the finite element method. The underlying premise of the method states that a complicated domain can be subdivided into a mesh in which the differential equations are approximately solved. By assembling the set of equations for each element of the mesh, the behavior over the entire problem domain can be determined.

In the present work, a structured mesh was created using algebraic interpolation methods, such as the Cox-De Boor formulation for the B-spline functions [27].

The mesh includes both parts (active and passive) of the myocardium using two different elements: a one-dimensional fiber element and an isoparametric hexahedrical tissue element of eight nodes. Both elements can be linked in the model by either coupling the nodes to their movement or directly sharing them to create a geometrical model in a manner similar to that proposed by Hedenstierna [28] (Figure 2). The main idea of element discretization is to divide the geometry (in this case the helical myocardium) in the various elements that are joined by the nodes. In this study, each fiber was created along the path of the band and divided into several fiber elements. The muscular tissue was created by dividing the band into several tissue elements.

2.6 The helical myocardium and its computational geometry

The helical heart anatomy has two loops: the basal loop (right ventricle and basal left ventricle) and the apical loop (descendent segment and ascendant segments). The apical loop is the driving force of the heart throughout the cardiac cycle and generates a twist-untwist motion of the ventricles through which the base and the apex rotate in opposite directions [8,29]. These movements have been confirmed by magnetic resonance imaging using radiographic implanted markers [30], magnetic resonance tagging [14,31,32], and speckle tracking echocardiography [33].

The spatial distribution of the myocardial segments that constitute the myocardium is shown in Figure 3. The geometry of the **helical myocardium** detailed in this figure was defined from medical imaging and graphic reconstruction techniques and was used to obtain the meshed model simplification. This geometry represents the silicone model of the helical myocardium (Figure 3.a): the fiber elements of the model are displayed in pink (Figure 3.b), and the connective tissue elements are shown in green (Figure 3.c).

To reconstruct the model, coronary CT angiographic examinations of the silicone model were performed using a 64-detector row scanner (Aquilion; Toshiba Medical Systems, Otawara, Japan) to obtain a digital image of the model (separation of each image slice, 0.5 mm). From this data, the fiber-based structure was created using the computer modeling software Rhinoceros®.

Comparative images (Figure 4) are also included in this paper to differentiate the parts of the model that correspond to each of the myocardial segments of the band to aid the understanding of the geometry of the simplified model.

2.7 Case study

Four different activation patterns were solved in the computational model. The difference between these patterns is the activation point from which the action potential starts propagating along the band (Figure 5). This point was generated by choosing a specific point in the model, and the wave was then propagated in a continuum way along the path described by the fibers.

- PATTERN 1: The action potential starts at the initial part of the right segment in the base near the pulmonary artery.
- PATTERN 2: The action potential starts at the initial part of the right segment in the base of the right ventricle and at a point at the beginning of the left segment in the basal free wall of the left ventricle to generate a dual-site stimulation.
- PATTERN 3: The action potential starts at the end of the ascendant segment in the upper portion of the interventricular septum.
- PATTERN 4: The action potential starts at the lower part of the septum.

Patterns 1 and 2 were proposed as the likely explanation for the observed phenomena, and patterns 3 and 4 were used as an alternative possibility of electromechanical propagation.

The equations in the simplified helical myocardium continuum model, which was meshed with 400 eight-node hexahedrical elements and 15 fibers inside, each of which was meshed with 50 two-node fiber elements, were solved. For the purpose of the present study, the results of the deformation part are not included

3 Results

Figure 5 shows the different activation times obtained along the geometry of the model when each pattern was solved. The activation time is the instant at which the action potential appears in this part of the band after its propagation along the band.

Pattern 1 shows that the action potential starts at the initial part of the right segment, i.e., at the base near the pulmonary artery, and reaches the end of the propagation the end of the ascendant segment (at the upper portion of the interventricular septum). Pattern 2 shows the action potential starting at the initial part of the right segment in the base of the right ventricle and at a second point in the beginning of the left segment (in the basal free wall of the left ventricle) and ending at the end of the ascendant segment. Pattern 3 shows the action potential starting at the end of the ascendant segment in the upper portion of the interventricular septum and ending at the initial part of the right segment. In addition, pattern 4 shows the action potential starting at the lower part of the septum and ending at the initial part of the right segment.

Figure 6 shows the vertical section of the simplified model of the propagation of the action potential for the computationally modeled propagation patterns 1, 2, 3, and 4. The different instants of time are labeled as A, B, C, D, and E and correspond to the labels A, B, C, D, and E in the image of the radionuclide angiocardiography [12], which provides information on the wavefront (indicated in yellow) of ventricular contraction. Ballester et al. [12] described that the earliest activation in radionuclide angiocardiography occurs at the base of the right ventricle, near the pulmonary infundibulum, and extends to the basal portion of the left ventricle. At the time of the mechanical activation of the base of the heart, the apex and septum appear to be spared, leaving an “island of inactivity” (white arrow). The results obtained for patterns 1, 2, 3,

and 4 can be compared with this observed wavefront in the radionuclide angiocardiography [19].

4 Discussion

Many research groups have exerted efforts in the design of mechanical and electrical models of the heart [17,23,34]. However, none of these models take into account the helical configuration of the ventricular myocardial fibers for the study of the electromechanical sequence. The present work is one of the first attempts that provides a computational model of the electromechanical propagation based on a simplified continuous helical ventricular anatomy.

The anatomic description of the helical ventricular structure that results in twist-untwist mechanics, as was elegantly shown in magnetic resonance studies using the magnetic resonance tagging technique, microcrystals implanted in the different segments of the ventricle, or speckle tracking echocardiography [32], prompts questions regarding the precise electromechanical sequence of ventricular activation. In the present study, the modeling of this activity was analyzed according to the helical anatomy.

In the model proposed in the present study, the stimulation site that produced the sequence of electromechanical propagation that best fits the existing imaging observations [4,5] corresponds to the base of the heart, and this stimulation propagates to the apex (patterns 1 and 2 in Figure 6), which is contrary to the hypothesized apex-to-base propagation.

Several different initial stimulation sites were tested. To obtain pattern 1, the stimulus was generated beneath the pulmonary artery and progresses in a anisotropic manner along the myocardial band to progressively involve the right, left, descendant, and ascendant segments [8]. Pattern 2 was established according to the findings from a

Fourier analysis of blood pool imaging [5] and magnetic resonance tagging studies [4,14], which observed two basal initial stimulation sites: the basal portion of the right ventricle and the basal free wall of the left ventricle. Pattern 3 assumed an electromechanical activation at the upper part of the septum, and the initial stimulation site in pattern 4 was placed at the apex.

The results reveal that the pattern that best fits the observations regarding the initial site and the sequence of electromechanical propagation are patterns 1 and 2, which favor a base-to-apex direction.

These results are apparently contradictory with the classical descriptions of the initial site and propagation of an electrical depolarization stimulus [1]. However, we have to take into account that these phenomena correspond to the electrification of the heart via the Purkinje system, which lasts a maximum of 80 ms and is represented by the QRS wave on the ECG. In fact, the Purkinje system, which is isolated from the surrounding myocardium [21], provides a fast means to electrify the ventricles prior to mechanical activation. In humans, the Purkinje system starts at the level of the atrioventricular (AV) node, branches via the right and left bundles, subendocardially spreads in a caudal way to the right and left ventricles, and then ascends toward the base of the heart, where it fades [35]. The QRS wave of the ECG corresponds to the electrical activation of the Purkinje system [1], and the direction of this type of electrification is from the apex to the base. It is logical to assume that the electrical stimulus delivered by the Purkinje system at the base of the heart then propagates according to the helical anatomy from the base to the apex, as observed in imaging studies [5], and this phenomenon lasts 300-400 ms, which corresponds to the ventricular systole.

Therefore, the present model supports previous observations of a base-to-apex electromechanical propagation of ventricular mechanical activity. The model may

provide a useful research tool to investigate the electromechanical patterns resulting from different stimulation sites, which would be useful in cardiac resynchronization therapy.

References

[1] D. Durrer, R. Van Dam, G. Freud, Total excitation of the isolated human heart, Circulation. 41 (1970) 899–912.

[2] C. Fish, Electrocardiography, Saunders, Philadelphia, 1997.

[3] P. Sengupta, V. Krishnamoorthy, Left ventricular form and function revisited: applied translational science to cardiovascular ultrasound imaging, Journal of the American …. 20 (2007) 539–551.

[4] B.T. Wyman, W.C. Hunter, F.W. Prinzen, E.R. McVeigh, Mapping propagation of mechanical activation in the paced heart with MRI tagging., The American Journal of Physiology. 276 (1999) H881–91.

[5] M. Ballester-Rodés, A. Flotats, F. Torrent-Guasp, M. Ballester-Alomar, F. Carreras, A. Ferreira, et al., Base-to-apex ventricular activation: Fourier studies in 29 normal individuals., European Journal of Nuclear Medicine and Molecular Imaging. 32 (2005) 1481–3.

[6] D. Sodi-Pallares, A. Bisteni, G.A. Medrano, F. Cisneros, The activation of the free left ventricular wall in the dog's heart, American Heart Journal. 49 (1955) 587–602.

[7] S.H. Gilbert, A.P. Benson, P. Li, A. V Holden, Regional localisation of left ventricular sheet structure: integration with current models of cardiac fibre, sheet and band structure., European Journal of Cardiothoracic Surgery Official Journal of the European Association for Cardiothoracic Surgery. 32 (2007) 231–249.

[8] F. Torrent-Guasp, M. Ballester-Rodés, G.D. Buckberg, F. Carreras, a Flotats, I. Carrió, et al., Spatial orientation of the ventricular muscle band: physiologic

contribution and surgical implications., The Journal of Thoracic and Cardiovascular Surgery. 122 (2001) 389–92.

[9] F. Torrent-Guasp, L. Dilatación, Estructura y función del corazón, Rev Esp Cardiol. (1998) 25–28.

[10] M. Ballester-Rodés, A. Ferreira, F. Carreras, The myocardial band., Heart Failure Clinics. 4 (2008) 261–72.

[11] F. Poveda, D. Gil, E. Marti, A. Andaluz, M. Ballester, F. Carreras., Helical structure of the cardiac ventricular anatomy assessed by Diffusion Tensor Magnetic Resonance Imaging multi-resolution Tractography, Rev Esp Cardiol. on press (n.d.).

[12] M. Ballester-Rodés, A. Flotats, F. Torrent-Guasp, I. Carrió-Gasset, M. Ballester-Alomar, F. Carreras, et al., The sequence of regional ventricular motion., European Journal of Cardio-thoracic Surgery : Official Journal of the European Association for Cardio-thoracic Surgery. 29 Suppl 1 (2006) S139–44.

[13] G.D. Buckberg, M.L. Weisfeldt, M. Ballester-Rodés, R. Beyar, D. Burkhoff, H.C. Coghlan, et al., Left ventricular form and function: scientific priorities and strategic planning for development of new views of disease., Circulation. 110 (2004) e333–6.

[14] A. Nasiraei-Moghaddam, M. Gharib, Evidence for the existence of a functional helical myocardial band., American Journal of Physiology. Heart and Circulatory Physiology. 296 (2009) H127–31.

[15] Dan Longo, A. Fauci, D. Kasper, S. Hauser, J. Jameson, J. Loscalzo, Harrison’s Principles of Internal Medicine, 17 h editio, McGraw-Hill, n.d.

[16] P. Libby, R.O. Bonow, D.L. Mann, D.P. Zipes, Braunwald’s Heart Disease: A Textbook of Cardiovascular Medicine, Saunders/Elsevier, 2011.

[17] N. Smith, C. Stevens, P. Hunter, Computational Modeling of Ventricular Mechanics and Energetics, Applied Mechanics Reviews. 58 (2005) 77.

[18] M. Sermesant, H. Delingette, N. Ayache, An electromechanical model of the heart for image analysis and simulation., IEEE Transactions on Medical Imaging. 25 (2006) 612–25.

[19] J. Marcé-Nogué, Understanding the Electro-mechanical Activation of the Myocardium, Journal of Basic and Applied Physics. 1 (2012) 16–23.

[20] A. Grosberg, M. Gharib, Physiology in phylogeny: modeling of mechanical driving forces in cardiac development., Heart Failure Clinics. 4 (2008) 247–59.

[21] H. Coghlan, A. Coghlan, The structure and function of the helical heart and its buttress wrapping. III. The electric spiral of the heart: The hypothesis of the anisotropic conducting matrix., Seminars in Thoracic …. 13 (2001) 333–341.

[22] F. Poveda, E. Martí, D. Gil, F. Carreras, M. Ballester, Helical Structure of Cardiac Ventricular Anatomy by Diffusion Tensor MRI Multi-â€• resolution Tractograpy, Journal of the American College of Cardiology. on press (2012).

[23] M. Sermesant, P. Moireau, O. Camara, J. Sainte-Marie, R. Andriantsimiavona, R. Cimrman, et al., Cardiac function estimation from MRI using a heart model and data assimilation: advances and difficulties., Medical Image Analysis. 10 (2006) 642–56.

[24] R.R. Aliev, A.V. Panfilov, A simple two-variable model of cardiac excitation, Chaos, Solitons & Fractals. 7 (1996) 293–301.

[25] D. Chapelle, F. Clément, F. Génot, P. Tallec, M. Sorine, J. Urquiza, A physiologically-based model for the active cardiac muscle contraction, Functional Imaging and Modeling of the Heart. 2230 (2001) 128–133.

[26] J.J.L. Emery, J.H. Omens, A.D. McCulloch, Biaxial mechanics of the passively overstretched left ventricle, American Journal of …. 272 (1997) H2299.

[27] E.T.Y. Lee, A simplified B-spline computation routine, Computing. 29 (1982) 365–371.

[28] S. Hedenstierna, P. Halldin, K. Brolin, Evaluation of a combination of continuum and truss finite elements in a model of passive and active muscle tissue., Computer Methods in Biomechanics and Biomedical Engineering. 11 (2008) 627–39.

[29] G. Buckberg, C. Clemente, The structure and function of the helical heart and its buttress wrapping. IV. Concepts of dynamic function from the normal macroscopic helical structure., Seminars in Thoracic …. 13 (2001) 342–357.

[30] N. Ingels, G. Daughters, E. Stinson, E. Alderman, Measurement of midwall myocardial dynamics in intact man by radiography of surgically implanted markers., Circulation. 52 (1975) 859–867.

[31] C. Lorenz, J. Pastorek, J. Bundy, Function: Delineation of Normal Human Left Ventricular Twist Throughout Systole by Tagged Cine Magnetic Resonance Imaging, Journal of Cardiovascular Magnetic Resonance. 2 (2000) 97–108.

[32] F. Carreras, J. Garcia-Barnes, D. Gil, S. Pujadas, C.H. Li, R. Suarez-Arias, et al., Left ventricular torsion and longitudinal shortening: two fundamental components of myocardial mechanics assessed by tagged cine-MRI in normal subjects., The International Journal of Cardiovascular Imaging. (2011).

[33] P. Sengupta, B. Khandheria, J. Narula, Twist and untwist mechanics of the left ventricle, Heart Failure Clinics. 4 (2008) 315–324.

[34] R.C.P. Kerckhoffs, S.N. Healy, T.P. Usyk, A.D. McCulloch, Computational Methods for Cardiac Electromechanics, Proceedings of the IEEE. 94 (2006) 769–783.

[35] D. Zipes, Genesis of cardiac arrhythmias: Electrophysiological considerations, Heart Disease: A Textbook of Cardiovascular Medicine, …. (1997) 550.

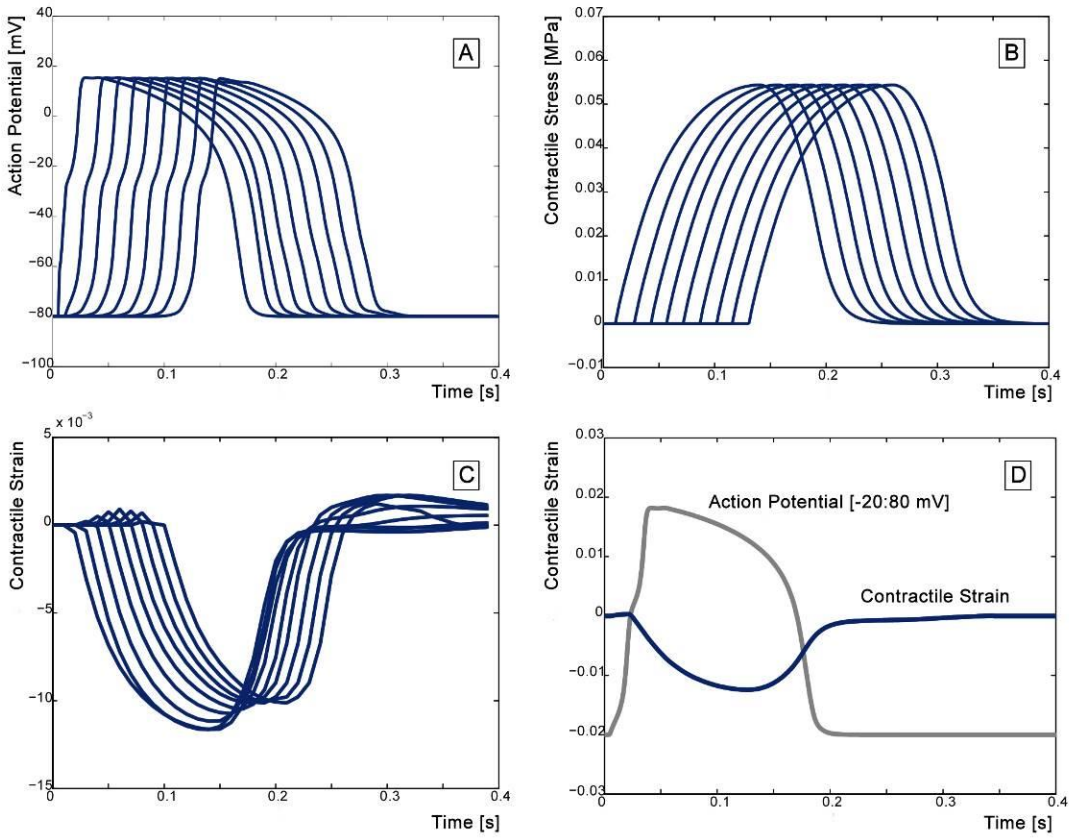

Figure 1 - Evolution of propagation of the (a) action potential, (b) contractile stress, and (c) contractile strain over time along the fibers. (d) Contractile strain of the fiber after activation of the action potential.

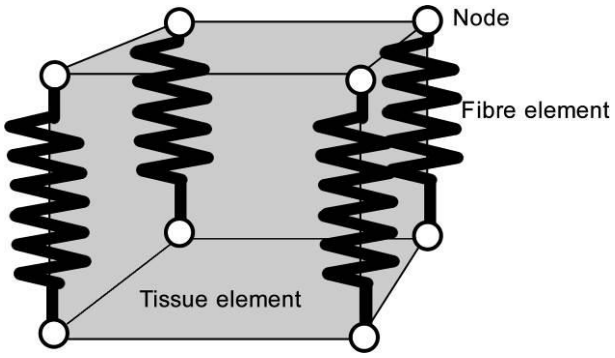

Figure 2 – Linked fiber and tissue elements to couple the active and the passive parts.

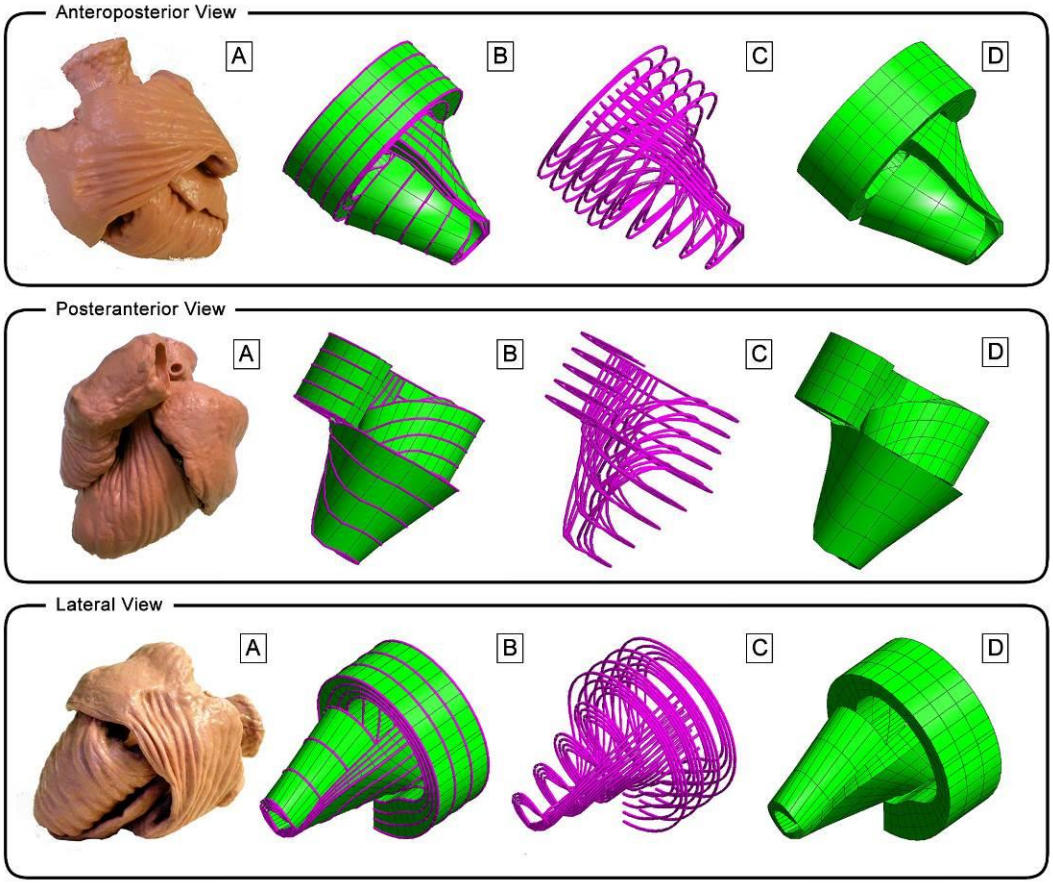

Figure 3 - Silicone (A) and finite element (B, C, and D) models of the helical myocardium. The finite element shows (B) the whole model with all of the elements, (C) only the fiber elements, and (D) only the tissue elements.

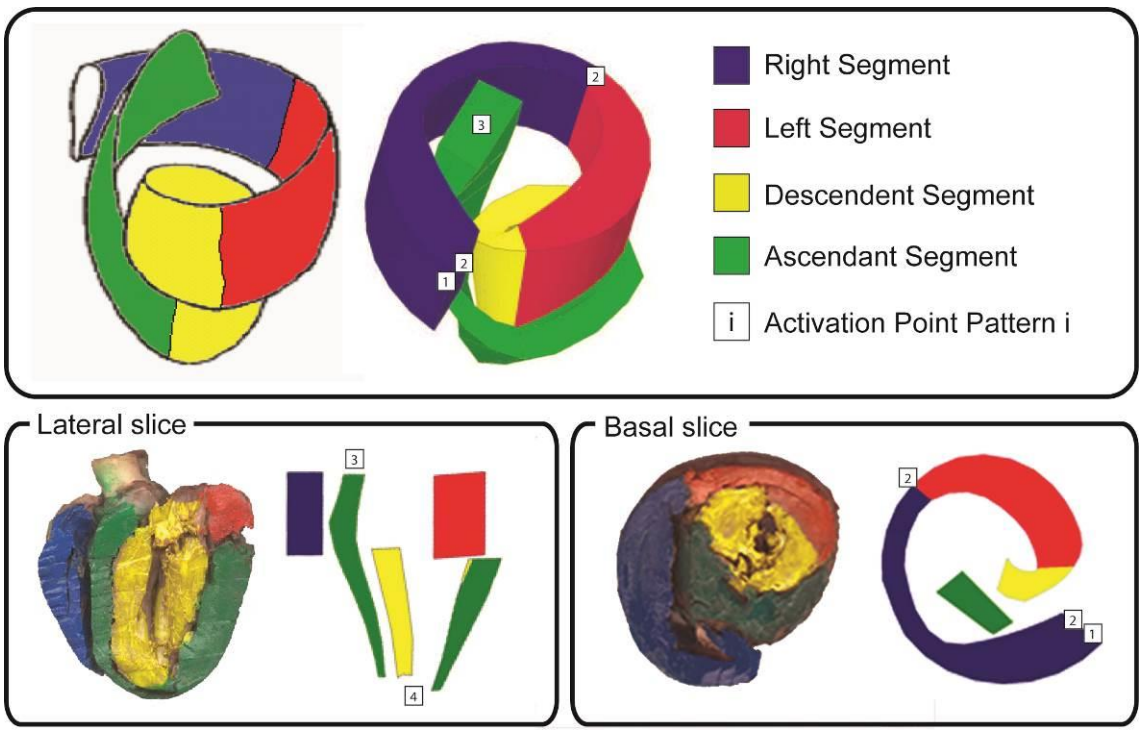

Figure 4 - The four differentiated segments in the model.

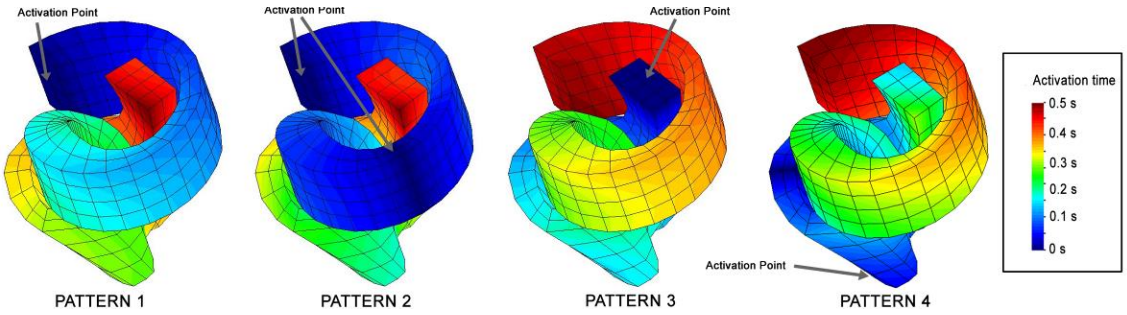

Figure 5 - Activation time depending on the activation pattern.

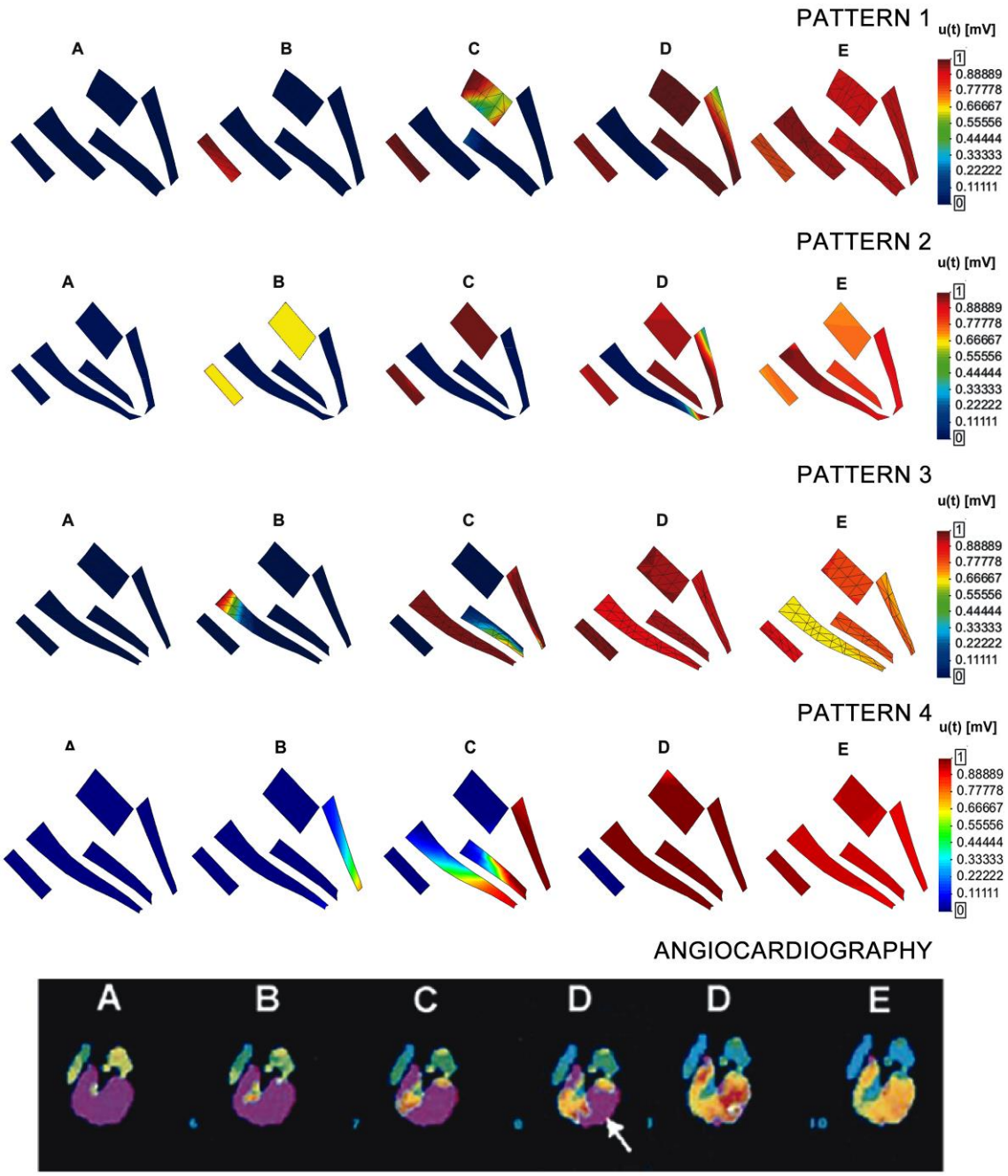

375

376 Figure 6 - Propagation of the action potential in patterns 1, 2, 3, and 4 and radionuclide

377 angiocardiography.

378